Interplay between hydrogen and vacancies in α-Fe

Erin Hayward and Chu-Chun Fu
CEA, DEN, Service de Recherches de Métallurgie Physique, F-91191 Gif-sur-Yvette, France
(Received 18 February 2013; revised manuscript received 19 April 2013; published 14 May 2013)

We present an atomistic study of the behavior and interactions of hydrogen and vacancies in body centered cubic (bcc) iron, using both *ab initio* and classical molecular dynamics methods. Hydrogen causes damage to materials through embrittlement, hardening, and swelling; we investigate the role of vacancies in these processes. Hydrogen, which normally diffuses with a very small barrier, is strongly trapped at monovacancies and vacancy clusters, resulting in changes to its electronic structure. Following saturation of the surface of a vacancy cluster, the formation of H_2 molecules is possible, at variance with the situation in the bulk. High local concentrations of hydrogen increase the likelihood of vacancy formation and stabilize vacancy clusters. Small hydrogen-vacancy clusters generally tend to diffuse by dissociation, but the trivacancy is shown to be capable of dragging hydrogen while migrating. We describe the structure of clusters of vacancies with varying hydrogen concentrations, finding that compact or spherical bubbles are generally lower energy than planar or linear configurations. Comparison with other bcc metals and with experiment is provided. For systems involving light elements such as hydrogen, corrections for zero-point energy are very important; we include these in our calculations and discuss their importance for different properties.

DOI: 10.1103/PhysRevB.87.174103 PACS number(s): 61.72.J−, 66.30.−h, 61.72.Qq, 31.15.A−

I. INTRODUCTION

Hydrogen is often present in structural materials used for a wide variety of applications. Its interaction with the lattice affects the microstructural evolution of the material and may present a serious problem, for example, for future fusion reactors. While hydrogen-assisted materials failure via embrittlement and corrosion is a well-documented phenomenon, the specific mechanisms responsible for these effects are still a matter of debate.

The most popular theories that seek to explain hydrogen embrittlement include hydrogen-enhanced decohesion (HEDE)[1] and hydrogen-enhanced local plasticity (HELP).[2] However, more recently, vacancy-assisted mechanisms have been proposed to be essential to the process.[3,4] Hydrogen atoms are thought to stabilize vacancies, leading to the growth of voids and bubbles and increased plasticity in the material.[5,6] This is clearly an important consideration for irradiated environments, where vacancies are abundant. However, even in systems with low equilibrium vacancy concentrations, hydrogen has been observed to induce the creation of substantial numbers of vacancies in a process called superabundant vacancy formation.[7,8] Thus, a fundamental understanding of the interactions between hydrogen and vacancies is needed. While bubbles have been seen during experimental analysis,[9–11] the details of the formation, growth, and agglomeration processes are difficult or impossible to observe *in situ*.

In this study, we choose body centered cubic (bcc) iron as a model element in which to study the interactions of hydrogen with the crystal lattice. This material is the main component of ferritic steels, which are widely used and desirable for their resistance to swelling and favorable thermal properties. Hydrogen is generally considered to have a very low solubility and rapid diffusion through iron.[12,13] Despite this, experiments show that its presence has a significant influence on mechanical properties, which can be associated with the trapping and accumulation of hydrogen at lattice defects.[4,14–16] Iron often behaves differently than the nonmagnetic bcc transition metals; for example, the ⟨110⟩ self-interstitial dumbbell is clearly the most stable configuration in iron, as opposed to the ⟨111⟩ configuration seen in other materials.[17] Thus, comparison of the behavior of hydrogen in iron with its behavior in other related materials is interesting and will be presented throughout the paper.

Several computational studies have addressed some of the relevant issues concerning hydrogen's behavior in iron, including bulk solution energy and site preference, bulk diffusion barriers, and binding to monovacancies, dislocations, and solutes.[5,18–24] However, there are still several open questions, in particular those which concern the interplay between hydrogen and vacancies. For example, how is the diffusion of hydrogen affected by vacancies, and vice versa? What is the low energy configuration of a hydrogen-vacancy cluster as a function of size? We approach these topics from several angles, paying close attention to the electronic interactions and quantum energy corrections for hydrogen. This paper is organized as follows: Sec. II presents our multiscale methodology. Section III A describes hydrogen diffusion in bulk Fe, while Sec. III B delineates how vacancy traps affect H diffusion and electronic structure. The potential for hydrogen atoms to cluster and induce vacancy formation is investigated in Sec. III C. Section III D describes how the diffusion mechanisms and barriers of vacancy clusters are changed by the presence of hydrogen. Finally, Sec. III E gives a description of the low-energy structures of hydrogen-vacancy clusters at a variety of sizes and introduces a general model for predicting the energy of bubbles with low hydrogen concentrations. An understanding of these topics gives insight into how bubbles form, diffuse, and contribute to hydrogen embrittlement.

II. METHODS

Ab initio calculations were performed within the density functional theory (DFT) framework, as implemented in the

TABLE I. Results of convergence testing for box size. H_T is a hydrogen tetrahedral interstitial; H_1V_1 refers to a single hydrogen atom in a monovacancy; V_4 ($\langle 111\rangle$ linear) and V_4 (compact) are quadruple vacancy clusters. We use k-point grids of $6 \times 6 \times 6$, $4 \times 4 \times 4$, $3 \times 3 \times 3$, and $2 \times 2 \times 2$ for 16, 54, 128, and 250 atom supercells, respectively. E_F is the formation energy of a configuration; E_B is the total binding energy of the configuration; ZPE gives the zero-point energy of the hydrogen atom in the given configuration; all three of these columns are given in eV.

Case	Supercell	E_f	E_B	ZPE
H_T	16	0.10		
	54	0.13		
	128	0.14		
	250	0.12		
H_1V_1	16	1.87	0.49	0.114
	54	1.82	0.49	0.118
	128	1.82	0.50	0.117
	250	1.81	0.50	
V_4($\langle 111\rangle$ linear)	54	24.14	0.40	
	128	24.15	0.41	
	250	24.20	0.41	
V_4 (compact)	54	7.52	1.18	
	128	7.51	1.21	
	250	7.53	1.23	

SIESTA code.[25] Calculations were spin-polarized within the collinear approximation and used the generalized gradient approximation (GGA) with the Perdew-Burke-Ernzerhof (PBE) exchange-correlation functional.[26] The GGA performs significantly better than the local density approximation (LDA) for iron systems; the latter does not predict the correct bcc ferromagnetic ground state.[27–29] Core electrons were replaced by nonlocal norm-conserving pseudopotentials, while valence electrons were described by linear combinations of numerical pseudo-atomic orbitals. The charge density was represented on a real-space grid of approximately 0.07 Å. The Methfessel-Paxton broadening scheme with a 0.3 eV width was used. Most calculations were performed at constant pressure, allowing for relaxation of all atomic positions and the volume and shape of the supercell. For simulations involving no vacancies or a monovacancy, a supercell of 128 atoms with a $3 \times 3 \times 3$ k-point grid was employed; for configurations with more than one vacancy, we used a 250 atom supercell with a $2 \times 2 \times 2$ k-point grid. The larger box size was necessary for some of the multivacancy cases with extended vacancy defects to ensure that the defect was fully enclosed in the simulation cell and not subject to fictitious interactions between self-images due to the use of periodic boundary conditions; it was employed in all multivacancy cases for consistency. Convergence testing was performed in several cases with results shown in Table I.

The pseudopotential and the basis set for Fe atoms have been shown to successfully capture the properties of self-defects in α-Fe and compare favorably to those found with DFT codes using plane wave basis sets.[30–32] While the basis for hydrogen is new to this work, it replicates the properties of the H_2 molecule well with a bond length of 0.75 Å and a vibrational frequency of 4263 cm^{-1} (compared to the experimental values of 0.41 Å and 4401 cm^{-1}).[33,34] The estimated error bar for the most relevant magnitudes reported below (such as the relative energy of two configurations and migration barriers) is around 0.05 eV.

Zero-point energy (ZPE) corrections are included in most of the DFT calculations, except where otherwise noted. Performing these calculations is expensive, but the corrections can be significant for hydrogen. To reduce the computational effort required for larger simulation cells, a $3 \times 3 \times 3a_0$ subset of the simulation cell was selected for this calculation; convergence testing assured us that these calculations are rather insensitive to box size (see Table I). We calculate the force constant matrix, or Hessian, by displacing each atom in the system by 0.04 Bohr in six directions. Although the responses of all atoms, both H and Fe, were considered when calculating the Hessian, only the eigenvalues which can be attributed to hydrogen atoms are used to calculate the ZPE corrections given in this work. Since the mass of iron is large compared to that of hydrogen, it has a negligible response to the displacement of hydrogen, and the contribution to the total ZPE correction due to Fe may be neglected within the Einstein approximation. This method of calculating the ZPE relies on the harmonic approximation, which may be inaccurate for hydrogen.[35,36] However, our calculated value for the ZPE of an H_2 molecule (0.28 eV) is very close to the value found by experiment[33] and by more exact methods such as configuration interaction (CI) of 0.27 eV.[34] Additionally, a DFT comparison of harmonic and anharmonic calculations for the ZPE of interstitial hydrogen in Al shows only small differences.[37] Thus, we judge the harmonic approximation to be sufficient at the level of precision of our calculations.

In addition to our DFT calculations, the LAMMPS molecular dynamics (MD) simulator[38] is used in conjunction with the embedded atom method (EAM) type potential[39] of Ramasubramaniam *et al.* for the Fe-H system.[40,41] Zero-point energy corrections were included in the original fit of this interatomic potential to DFT data. Combined with Monte Carlo (MC) steps, we are able to efficiently search for low energy configurations of clusters that can be used as input for SIESTA. In the MDMC method, we begin with a supercell of 2000 Fe atoms ($10 \times 10 \times 10a_0$). The vacancy cluster of the desired shape and size n is placed in the center, then m hydrogen atoms are randomly introduced into the void. After an initial minimization of the entire system is performed using the LAMMPS molecular dynamics simulator,[38] the iterative process begins: Each hydrogen atom is then moved randomly by up to 0.8 Å in each of the x, y, and z directions, and the system energy is minimized. The energy of this new state is compared to that of the previous state, with selection criteria based on the Metropolis MC algorithm.[42] If the new state is lower in energy, it is selected, while if it is higher is energy, it is selected with a probability $p = \exp(\Delta E/kT)$, where k is Boltzmann's constant, and T is chosen to be 300 K. This allows the system to avoid becoming stuck in local energy minima. After at least 1000 iterations during which no new global energy minima are found, the process is complete. For more details, see Ref. 5.

Migration barriers and paths are determined using a two-step process. First, the climbing image nudged elastic band (CI-NEB)[43] is used with LAMMPS to efficiently search for diffusion pathways. Then the drag method, chosen for its

TABLE II. Solution energy of hydrogen interstitials (eV), as calculated by Eq. (1) (DFT data). We show the uncorrected value for solution energy (E_{sol}), the zero-point energy which can be attributed to the hydrogen atom when in the interstitial configuration, and the ZPE corrected values of solution energy. The reference state (a H_2 molecule) has a ZPE of 0.14 eV/H.

	T site	O site
Uncorrected E_{sol}	0.13	0.27
Interstitial zero-point energy	0.24	0.12
Corrected E_{sol}	0.23	0.26

computational efficiency, is used with SIESTA to get a more accurate value for the barrier height along the path found by CI-NEB. In this method, a series of hyperplanes are constructed between the initial and final configurations; all atoms in the system are allowed to relax in plane.[31,44,45] These calculations are performed at constant volume. Many images are chosen between the initial and final states to verify the path, although we calculate the ZPE correction only at the minima and the transition state.

This coupling of molecular dynamics and DFT allows for the efficient and accurate simulation of a wide range of system sizes and configurations. Additionally, it serves as a test of the empirical potential as an appropriate tool for describing the behavior of hydrogen in many scenarios.

III. RESULTS

A. Hydrogen in solution and diffusion in perfect bulk

The bcc lattice has two possible high-symmetry interstitial sites: the tetrahedral site (T site) and the octahedral site (O site). As has been found in the majority of previous computational studies in Fe, we find that a single hydrogen atom preferentially resides in T site in bcc Fe.[18,19] Experimental results also indicate that at low temperature hydrogen will reside predominantly at T sites, with O-site occupation becoming notable only at high temperature.[12,46] This result is typical of bcc transition metals, including tungsten,[47–49] vandium,[50] niobium,[51] and tantalum.[51]

Before correction for zero-point energy, the O site is approximately 0.14 eV higher in energy than the T site, in good agreement with results from previous studies.[19] Values for the solution energy or interstitial formation energy are given for each interstitial site in Table II, with and without ZPE corrections. We use the formula

$$E_{sol} = E(H_{int}) - E_0 - \tfrac{1}{2}E(H_2), \quad (1)$$

where the reference state is an H_2 molecule in vacuum, which has a zero-point energy of 0.14 eV/H, and a block of pure iron with energy E_0 of the same size as the supercell containing the hydrogen interstitial defect. Vibrational analysis shows that the T site is a true minimum, while the O site is a second order stationary point;[19] thus, the ZPE correction for the T site is larger than for the O site. With inclusion of the zero-point energy correction, the value for solution energy agrees well with previously quoted experimental[52] and computational values,[18,19,24,53] which range from 0.20 to 0.32 eV.

TABLE III. DFT diffusion barriers for hydrogen in the bulk, eV.

	T → T	T → O → T
Uncorrected barrier	0.090	0.148
Transition state ZPE	0.190	0.123
Corrected barrier E_a	0.044	0.035

Hydrogen can diffuse between T sites through two possible paths: directly between nearest neighbor T sites in a [110] direction (with the path curved towards an O site), or by crossing an O site in a [100] direction. Before ZPE corrections are considered, the T → T path is energetically preferable to the T → O → T path. However, as with the solution energy, inclusion of ZPE corrections proves to be significant, lowering the barrier (i.e., the activation energy E_a) in each case. As is shown in Table III and Fig. 1, the T → O → T path becomes a viable, and very low barrier, transition pathway. Considering the precision of our calculations, both barriers are essentially equivalent and quite small. The tested EAM potential produces barriers of the same magnitude, giving barriers of 0.040 and 0.049 eV for the T → T and the T → O → T paths, respectively. We note that a similarly low barrier of 0.042 eV for the T → T path has been reported.[19]

Given the low barriers, H migration can be considered as thermally activated only at low T. Applying quantum corrections to harmonic transition-state theory (TST),[54–56] diffusion occurs with the temperature dependent jump frequency Γ given by

$$\Gamma = \frac{k_B T}{h} \exp(-E_a/k_B T), \quad (2)$$

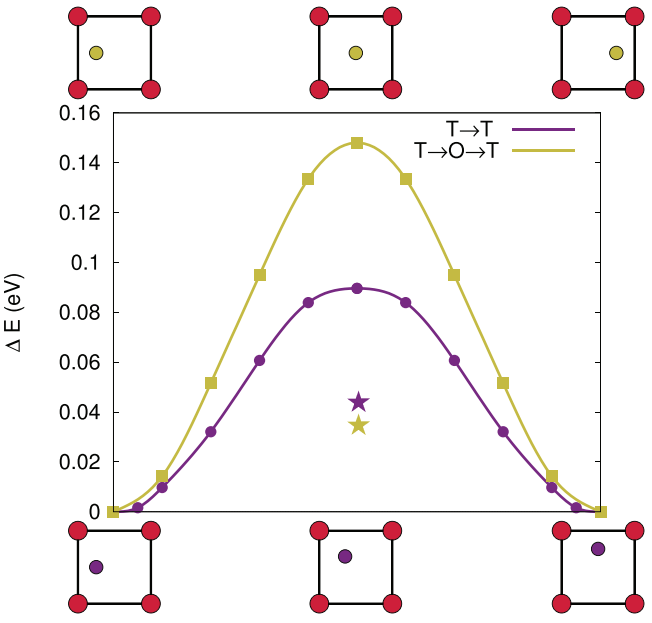

FIG. 1. (Color online) Barriers to the two possible paths for hydrogen diffusion in the bulk, from DFT calculations. Curves are uncorrected for zero-point energy (ZPE), while stars (of corresponding color) indicate the barrier height after the ZPE correction. The initial, transition state, and final configurations in the {100} plane are shown for each path.

TABLE IV. Diffusion coefficients D ($\times 10^{-8}$) [$m^2\ s^{-1}$] calculated at three temperatures T from Eqs. (2) and (3), based on DFT data. Experimental values come from Refs. 13, 46, and 61.

	278 K	318 K	350 K
T → T	0.76	1.09	1.39
T → O → T	0.92	1.28	1.58
Experiment	0.62–0.85	0.84–1.06	1.02–1.24

where E_a is the activation energy of jump, calculated using zero-point energy corrected values. Then, the diffusion coefficient is simply

$$D = \frac{na^2}{6}\Gamma, \tag{3}$$

where n gives the number of possible jump directions (four for the T → T and two for the T → O → T path) and a is the jump length. This derivation is intended to account for the discrete and widely spaced energy levels of hydrogen, but neglects tunneling effects. A transition state is generally defined to be a stationary point with one and only one negative eigenvalue, i.e., a saddle point of rank one.[57] However, it has been shown that stationary points of higher rank may be valid transition states as well, provided that they meet certain criteria, such as being sites of high symmetry or having degenerate negative eigenvalues.[58,59] Such a stationary point may connect more than two potential wells. This is the case for the O site, which is a second-rank stationary point from which any of four T sites are equally accessible. Thus, we assume the validity of TST for describing both paths.

There is scatter in the experimental data on hydrogen diffusion in Fe, due to differing material and experimental conditions;[60] however, our results generally compare quite favorably. In Table IV, we give a comparison of diffusivity values with three experimental papers (one of which is a review of several studies) at three temperatures near room temperature.

B. Hydrogen trapping at vacancies

Vacancies can act as strong traps for hydrogen diffusing through the bulk. Instead of preferring the T site, a hydrogen atom trapped at a vacancy occupies a position slightly offset from an O site neighboring the vacancy. These different environments result in changes to the electronic structure of the hydrogen and neighboring iron atoms, with a delocalization in energy accompanying a delocalization in space. These changes can be observed in the projected density of states (PDOS) graphs and differential charge density maps (the difference between the self-consistant charge density and the superposition of atomic densities) displayed in Figs. 2 and 3. When in the T site (or O site, which displays a very similar PDOS), weak hybridization of the s band of the hydrogen atom with the neighboring iron is reflected by an overlap of the low energy peaks, combined with a decrease in height and localization of Fe's d band. At the monovacancy, the delocalization of the hydrogen peak is quite significant, despite the decreased coordination of the H atom compared to in the bulk. A similar change was seen for H in Mo.[62] Additionally,

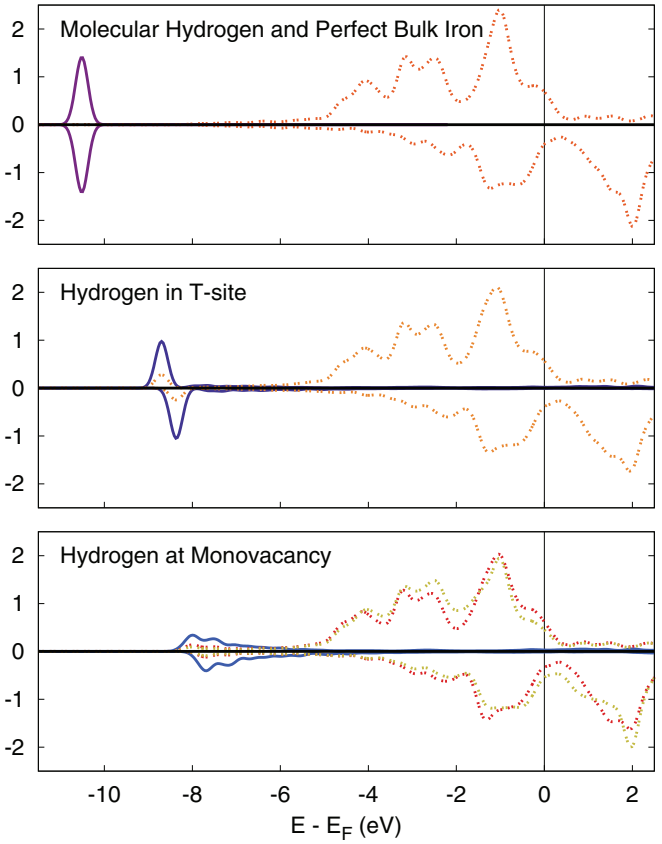

FIG. 2. (Color online) The projected density of states (PDOS) for a hydrogen atom (dark solid lines) and an iron atom (light dashed lines) in different environments. In the top graph, the hydrogen (in a H_2 molecule) and the iron are completely noninteracting. In the lower two graphs, the PDOS of iron is for atoms neighboring the hydrogen defects.

stronger hybridization with surrounding iron is seen. The corresponding charge transfer to the vacant lattice site and the neighboring iron atoms can be observed (Fig. 3), as well as loss of the spherical shape of the charge contour. While Fe is strongly ferromagnetic, Mulliken population analysis indicates that the local magnetic moment of hydrogen either in the interstitial T site or at a monovacancy is extremely weak, at -0.05 and $-0.08\ \mu_B$, respectively. The presence of hydrogen does not significantly alter the local magnetic moment of nearby iron atoms: in the bulk, a small drop is seen adjacent to the H interstitial, from the bulk value of 2.31 μ_B to 2.25 μ_B; a local magnetic moment of 2.54 μ_B is seen near a monovacancy, with or without hydrogen.

Several hydrogen atoms can be trapped at a monovacancy. Different bcc transitions metals have been shown to trap different amounts of hydrogen, with differing minimum energy configurations.[22,63] We tested several different configurations of up to six hydrogen atoms to determine the lowest energy states, which are pictured in Fig. 4.

A single hydrogen atom at a monovacancy resides in a position slightly offset from an O site towards the vacancy. The second hydrogen atom occupies the opposing O site. Four hydrogen atoms preferentially occupy O sites in the shape of a tetrahedron;[23] this state is about 0.1 eV lower in energy

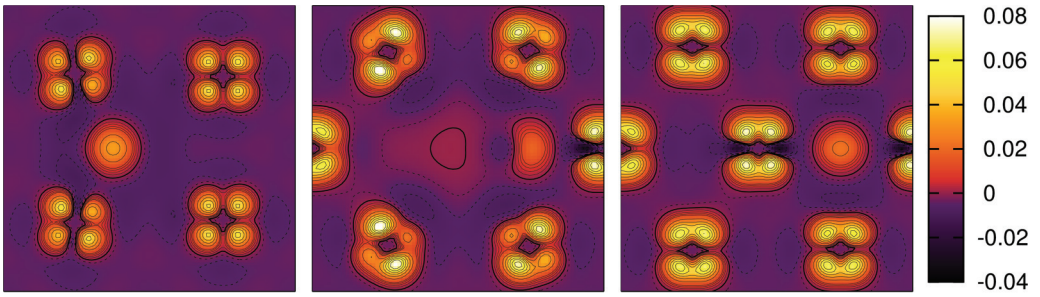

FIG. 3. (Color online) Differential charge density maps. All use the same scale, given in electrons/bohr^3. Isolines are given at intervals of 0.0025 between −0.01 and 0.01, and every 0.01 outside that range. Positive lines are solid, negative are dotted, and the thick lines denote 0.0 electrons/bohr^3. (a) H interstitial in a T site; view of the (1 0 0) plane. (b) H at a monovacancy, with the (1 1 0) plane that includes both the vacancy (center) and the hydrogen in the offset O site (right of center). (c) Same view as in part (b), but without the vacancy; the H interstitial is in the O site in perfect bulk Fe. Dimensions of all plots are 10.88 × 10.88 bohr.

than a planar configuration. In the H_6V cluster, we find that two hydrogen atoms remain on opposing O sites, while the other four relax to near T sites. This configuration is nearly energetically degenerate with the configuration in which all H atoms are near O sites.

To characterize each state, we calculate two different types of hydrogen binding energy. The first is incremental binding energy, that is, the binding energy of the mth hydrogen atom to the $H_{m-1}V$ cluster:

$$E_B^{\text{inc}} = [E(H_{m-1}V) + E(H_T)] - [E(H_mV) + E_0]. \quad (4)$$

This value is useful for determining the kinetic viability of the state in question: once a cluster containing m vacancies has been formed, is it possible to add the $(m+1)$-th to the cluster? Table V gives these incremental binding energies, both from this work and from previous studies. During vibrational analysis, we found that negative eigenvalues begin to appear at $m = 6$, indicating a slight instability in this configuration; also, the binding energy is extremely close to zero. Thus, we do not consider the addition of more hydrogen atoms. Our results are in good agreement with previous *ab initio* studies available in the literature, which show that no more than six hydrogen atoms may be exothermically bound to the monovacancy in bcc Fe.[18,22,23] We note that our calculations were performed in a 128-atom supercell, as opposed to the 54-atom cell often used.[18,23]

One can also define an average binding energy for all of the hydrogen atoms in the monovacancy:

$$E_B^{\text{avg}} = \frac{1}{m}[E(H_0V) - E(H_mV)] + E(H_T) - E_0. \quad (5)$$

After looking at the projected density of states for each hydrogen atom in an H_mV cluster (see Fig. 4), it becomes clear why this definition is relevant. Multiple hydrogen atoms occupy symmetric positions, have identical PDOS curves,

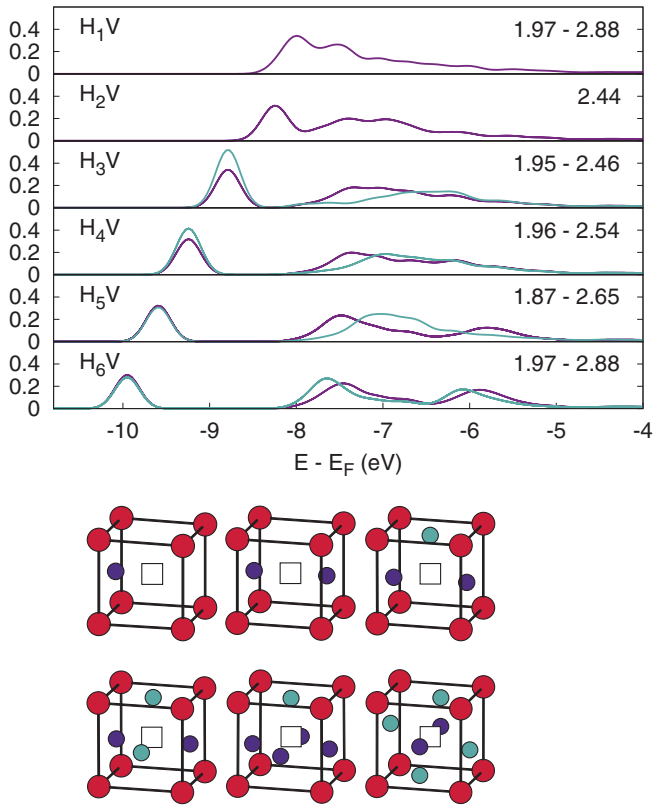

FIG. 4. (Color online) Projected density of states (PDOS) and structures of multiple hydrogen atoms at a monovacancy in the bcc Fe cell. Iron atoms are shown in red; hydrogen atoms are purple or teal, corresponding in color to the PDOS (only spin-up shown) graphs above; the vacancy is indicated by the square in the center of the cell. The minimum and maximum distance between two hydrogen atoms (Å) is shown in the right of each graph.

TABLE V. DFT values for the incremental binding energy of the mth hydrogen atom at a monovacancy in eV [see Eq. (4)]. Binding energies before correction for zero-point energy are shown in parentheses. For comparison, results from two previous *ab initio* studies are given.

m	E_B^{inc}	Ref. 23	Ref. 18
1	0.616 (0.498)	0.584	0.559
2	0.651 (0.543)	0.607	0.612
3	0.381 (0.337)	0.384	0.399
4	0.351 (0.304)	0.343	0.276
5	0.269 (0.269)	0.297	0.335
6	0.045 (−0.043)	0.002	−0.019

TABLE VI. DFT values for the average binding of energy of m hydrogen atoms at a monovacancy in eV [see Eq. (4)]. ZPE corrected binding energies and results from experiment are shown for comparison.

m	E_B^{avg}	Ref. 65
1	0.62	0.63
2	0.63	0.63
3	0.55	0.43
4	0.50	0.43
5	0.45	0.43
6	0.39	0.43

and thus have equivalent electronic interactions with the surrounding atoms. So once the low energy configuration has been reached (regardless of how it came to exist), it is not valid to say, for example, that the first hydrogen atom is significantly more well bound than the fifth. Then, the average binding energy defined in Eq. (5) becomes a more relevant number to describe the environment felt by any individual hydrogen atom. Although not all positions are symmetrically equivalent, there are at most two different symmetric positions in any cluster, which are differentiated by differently colored atoms and PDOS curves in Fig. 4. The values for average binding energy are given in Table VI, along with comparison to experiment.[64,65] In this ion-beam experiment, two main deuterium (D) desorption stages were observed after reaching conditions under which all of the D should have been trapped at lattice defects. The small discrepancies between our results and experiment can be attributed to the fact that our definition of average binding energy does not account for the slight differences between nonsymmetrically equivalent positions: for example, in the H_3V, one of the hydrogen atoms sees a different environment than the other two; additionally the ZPE of D can be expected to be slightly lower than that of H.

Figure 4 also gives the minimum and maximum distance between any two hydrogen atoms in the monovacancy, with the minimum distance between any two hydrogen atoms equal to 1.9 Å. As more hydrogen atoms are added to the cluster, the PDOS curves of the hydrogen atoms change. The s band splits into two distinct peaks, with a larger splitting corresponding to a weaker binding of the system. Additional splitting of the higher energy peak can be seen in the systems with the most hydrogen.

The formation of H_2 molecules within bubbles has been proposed to explain anomalously large measurements of hydrogen retained in irradiated steel.[11] Our DFT simulations show a clear tendency of hydrogen to hybridize with iron, and H_2 molecules introduced into the center of monovacancies always dissociate.[18] A nine-vacancy spherical cluster is taken as a test case for larger bubbles; the H_2 molecule is not stable here either. However, as more hydrogen is introduced to a cluster, and the surface saturates with hydrogen, there may be the opportunity for stable molecules to form in the center. Molecular dynamics with an EAM potential is ill-suited to answer this question: as the cluster surface is saturated, excess hydrogen is released into the bulk.[5] This is due to the inability of the EAM formalism to accurately describe H_2 molecules.

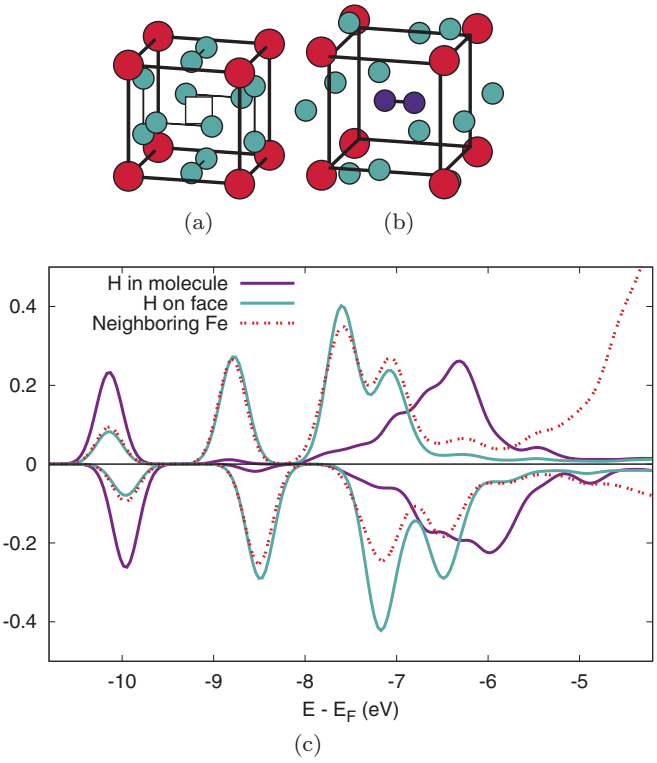

FIG. 5. (Color online) Oversaturated monovacancy: (a) The $H_{12}V$ configuration before minimization. (b) The fully minimized $H_{12}V + H_2$ [1 0 0] configuration. (c) The projected density of states (PDOS) for hydrogen in the molecule and on the face, and neighboring iron. Atoms are colored following the conventions in Fig. 4. PDOS curve colors correspond to the coloring of the atoms in parts (a) and (b).

This question can be addressed using DFT, albeit only for very small voids.

Although is unclear how such a configuration would come to exist, we oversaturate a monovacancy, placing two hydrogen atoms in opposing T sites on each face of the cell surrounding the vacancy, as shown in Fig. 5(a). Following minimization, a H_2 molecule (in either the [1 0 0], [1 1 0], or [1 1 1] orientation) is introduced to the center of the cell and further minimization is conducted [Fig. 5(b)]. The average binding energy of the system is slightly positive, indicating that this configuration is preferable to the hydrogen being distributed in the bulk as interstitials. We find that the molecule is stable, with the three tested orientations being energetically degenerate. Thus, rotation of the molecule may occur with a very small energy barrier. Giving evidence for the true molecular nature of these two hydrogen atoms, the equilibrium bond length is 0.76 Å, extremely close to the value in vacuum, and much shorter than the closest distance between any two hydrogen atoms observed in the bulk or in the undersaturated monovacancy (∼1.9 Å, as discussed below). Additionally, the PDOS curves of the hydrogen presumed to be in molecular form differ significantly from the PDOS curves of the hydrogen atoms on the surfaces of the vacancy, which show strong hybridization with the neighboring iron [Fig. 5(c)]. The PDOS of the molecular hydrogen displays a double-peaked structure: the lower energy peak is due to a strengthening of the signature molecular peak, while

the higher energy peak arises from weak interactions with hydrogen atoms on the surface. Finally, the Mulliken atomic population matrix indicates that there is significant charge accumulation, proportional to the bond orders,[66] between the two hydrogen atoms forming the molecule (and negligible accumulation with other hydrogen atoms), indicating a strong bond; the hydrogen atoms on the face show non-negligible bond order only with neighboring iron atoms.

Based on these results, we propose two regimes of interest for hydrogen bubbles: an undersaturated regime, in which the hydrogen atoms coat the surface of the bubble and interact primarily with nearby iron atoms; and a saturated regime, in which further introduction of hydrogen atoms results in the formation of molecules in the center of the cluster. In large saturated clusters or cavities, containment of multiple H_2 molecules should be possible.

C. Hydrogen clustering and vacancy formation

The clustering of hydrogen atoms in the bulk may affect the local stress of the lattice and induce vacancy formation. To investigate this possibility, we placed two hydrogen atoms at T sites various distances apart and allowed the entire system to relax. We calculate the binding energy between the atoms i and j at a distance of r using

$$E_B = 2E(\mathrm{H_T}) - [E(\mathrm{H}_i\mathrm{H}_j) + E_0], \tag{6}$$

where $E(\mathrm{H}_i\mathrm{H}_j)$ is the energy of the system containing two hydrogen atoms at a distance of r, E_0 denotes the energy of the system containing perfect bulk iron, and $E(\mathrm{H_T})$ is the energy of a system containing a hydrogen interstitial in the tetrahedral position; all three systems contain the same number of Fe atoms. With this convention, negative binding energies indicate a repulsion between atoms.

We find a strong repulsion between hydrogen atoms placed very near each other, followed by a sharp drop-off to weaker interactions at larger distance; the binding energies of the weak interaction regime are detailed in Fig. 6. During relaxation, atoms placed nearer to each other than ∼1.9 Å moved apart until this distance is obtained. This is the equilibrium distance for several configurations: the binding energy varied between these configurations, but is always repulsive, ranging from −0.31 eV for H atoms initially in nearest neighbor T sites to −0.05 eV for atoms on different faces of the unit cell. We find very slightly positive or zero binding energies at relaxed distances between 2.0 and 2.6 Å, followed by an increase in repulsion until the atoms were separated by 3.2 Å. After this distance, the binding energy goes to zero, as the atoms became increasingly separated. We note that the magnitude of these weaker binding energies is within the error of the calculations: in general, binding can be considered very weak to nonexistent at distances greater than about 1.9 Å in the bulk. As can be seen in Fig. 6, this corresponds to a significant change in the PDOS for the hydrogen atoms. At small separation distances, two distinct peaks are observed; qualitatively, when the peaks are closer together, the binding energy tends to be greater. These peaks merge at a distance of 3.2 Å, and as the separation distance increases further, a single peak is formed, equivalent to the PDOS of a H atom in the tetrahedral interstitial site. Our results are strikingly quantitatively similar to those obtained in

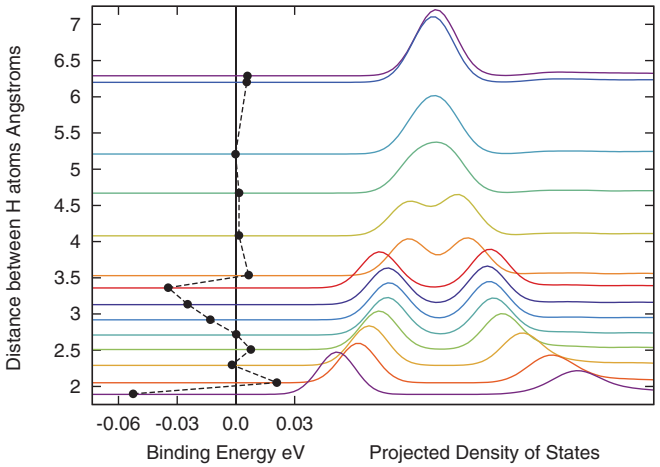

FIG. 6. (Color online) The binding energy [Eq. (6)] and spin-up projected density of states (PDOS) of a pair of weakly interacting hydrogen atoms in bulk iron. Spin-down PDOS is not shown for clarity, but the curves are nearly identical to their spin-up counterpoints. The y axis shows the distance between the two H atoms after relaxation.

simulations of vanadium.[50] As has been shown in the closely related bcc transition metals vanadium[50] and tungsten,[63] in iron, the most favorable orientation between H atoms in T sites is alignment along the [1 1 0] direction, at a distance of between 2.0 and 2.2 Å.

The formation energy of a vacancy in the vicinity of m clustered hydrogen atoms can be approximated with the following equation:

$$E_V^f = E(\mathrm{H}_m\mathrm{V}) - \frac{N-1}{N}E_0 - m[E(\mathrm{H_T}) - E_0], \tag{7}$$

where N is the number of iron atoms in the perfect cell with energy E_0. This equation does not explicitly account for any energy changes due to the clustering of multiple hydrogen atoms. However, these corrections are expected to be small, based on our results for H-H clustering in the bulk. As is shown in Fig. 7, the formation energy of a vacancy decreases

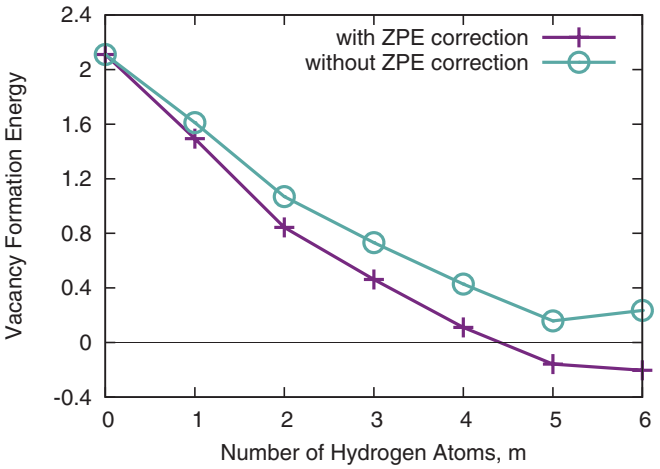

FIG. 7. (Color online) The DFT formation energy (eV) of a vacancy in the vicinity of clustered hydrogen atoms, as defined in Eq. (7), with and without zero-point energy (ZPE) correction.

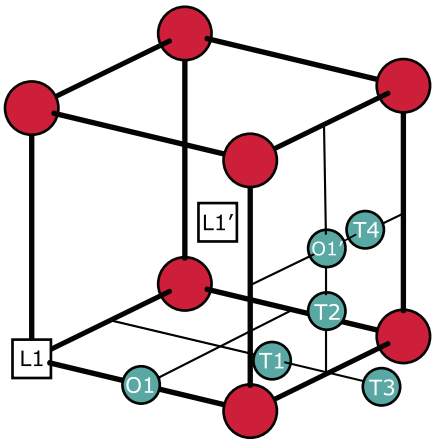

FIG. 8. (Color online) Schematic of positions relevant to hydrogen diffusion near a vacancy located at L1, with an iron atom at position L1′. Iron positions are shown in red; hydrogen positions are shown in teal. In the bound state, a vacancy resides on lattice position L1 with the hydrogen atom in position O1; an equivalent bound state which can be reached by migration of the cluster is denoted by L1′-O1′.

significantly as the hydrogen concentration increases, even becoming negative when ZPE corrections are included. With the minimum distance between any two hydrogen atoms in the bulk being smaller than a lattice spacing, an iron atom has a strong possibility of seeing high local H concentrations; this lends credence to the idea of super-abundant vacancy formation.[7,8]

D. Diffusion of hydrogen-vacancy clusters

In the bulk, a hydrogen atom in a tetrahedral site has four possible equivalent jumps to nearest-neighbor T sites, and two equivalent jumps across O sites. In the presence of a vacancy, this symmetry is broken, and these jumps are no longer necessarily energetically equivalent. We investigate possible jumps in the vicinity of the monovacancy, based on the configurations shown in Fig. 8. Both forward and reverse diffusion barriers are given in Table VII. Only the O sites directly adjacent to the vacancy are stable; hydrogen occupies T sites otherwise. For a single trapped hydrogen atom to dissociate from a monovacancy (configuration O1–L1), it must jump to the nearby T site T1. Further jumps away can proceed via the T → T path (T2) or the T → O → T path (T3). Reverse barriers and barriers to symmetrically identical states tend to be lower than barriers away from the vacancy, allowing for the possibility of retrapping. Although there is some variation in barrier heights between T sites with different relationships to the vacancy, barriers are generally on the order of the bulk values (less than 0.1 eV).

Corrections for ZPE are significant. In the case of the initial jump away from the bound state, the barrier is increased by 0.08 eV. This is because in the bound state, the ZPE due to hydrogen is quite low at 0.12 eV, compared to the bulk value of 0.24 eV; the transition state has a ZPE of 0.20 eV. However, for jumps between T sites near the vacancy, the ZPE correction lowers the diffusion barrier by roughly 50%. Corrections for the saddle points of the T1 → T2 and T1 → T3 transitions were calculated explicitly and were found to be nearly identical to the bulk values given in Table III. Thus, calculations of barriers further from the vacancy can safely be assumed to have the same magnitude of correction.

Vacancies diffuse through the bulk by jumping to nearest neighbor sites. In the case of a monovacancy, this barrier is 0.69 eV; jumps directly to second nearest neighbor sites are much less likely, with a barrier of 2.53 eV. Fu *et al*. found that migration of small vacancy clusters can proceed with lower barriers than the migration of monovacancies.[30] We find barriers similar to theirs, at 0.70, 0.25, and 0.47 eV for the V_2, V_3, and V_4 clusters, respectively.[30] While the V_2 and V_4 clusters require two consecutive nearest-neighbor jumps to recover equivalent low-energy configurations (see Ref. 30), the trivacancy does not. Additionally, the barrier to V_3 motion is quite low, at less than half the monovacancy diffusion barrier, making this a particularly interesting configuration. To investigate the effect of hydrogen on vacancy diffusion and to determine whether clusters of hydrogen and vacancies can migrate together or whether dissociation will occur, we introduce hydrogen into the monovacancy and trivacancy clusters.

When a hydrogen atom is trapped at a monovacancy, the vacancy sees an increased jump barrier at 0.76 eV (0.79 eV uncorrected for ZPE). The barrier for hydrogen to escape is lower at 0.64 eV. Once the hydrogen atom has made several jumps away from the vacancy, there is the possibility for the vacancy to jump and recover the bound state with a reduced barrier of 0.17 eV (0.29 eV uncorrected for ZPE); this series of events is depicted in Fig. 9. The first few steps of either complete dissociation or migration as a whole are identical—the hydrogen becomes detrapped from the vacancy and makes several jumps. Even with the reduced vacancy jump barrier available at this point, further dissociation of the hydrogen is much more likely with a barrier of only ∼0.04 eV. Based

TABLE VII. DFT diffusion barriers for hydrogen near a vacancy, eV. Columns give the initial positions and rows give the final positions. Along the diagonal, barriers are between symmetrically identical neighboring positions. See Fig. 8 for a diagram of the positions. Barriers given in parentheses are uncorrected for zero-point energy (ZPE).

	O1	T1	T2	T3	T4
O1	0.218 (0.215)	0.033 (0.078)			
T1	0.640 (0.554)	0.047 (0.101)	0.049 (0.091)	0.036 (0.146)	
T2		0.065 (0.122)	0.022 (0.060)	0.048 (0.097)	0.030 (0.068)
T3		0.081 (0.195)	0.079 (0.118)		
T4			0.004 (0.042)		

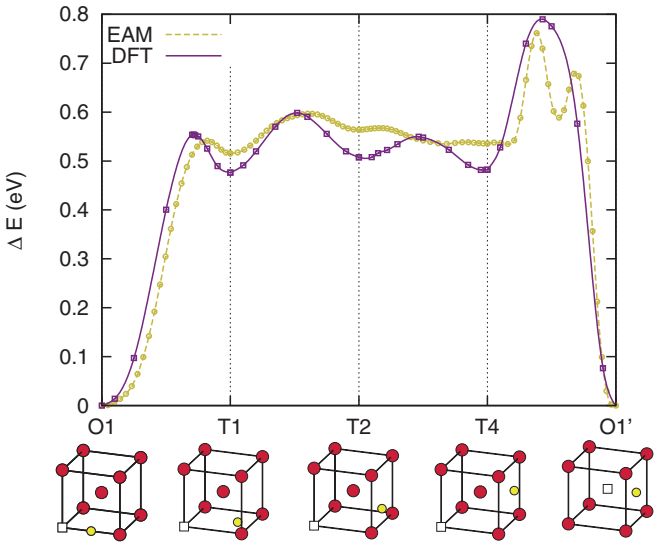

FIG. 9. (Color online) The uncorrected barriers to diffusion of a hydrogen-vacancy pair are shown, with stable configurations diagramed below. Results from the EAM potential are shown in yellow, results from the DFT are shown in purple. See Table VII for the ZPE corrected barriers.

on the total dissociation barrier of 0.64 eV and the coherent migration barrier of 0.76 eV, we conclude that the migration of hydrogen-vacancy pairs is not a viable mechanism by which small clusters may agglomerate into bubbles.

The diffusion of a H_1V_3 clusters has several interesting differences as compared to the H_1V_1 cluster. As in the monovacancy case, placing a hydrogen atom into the cluster increases the barrier for a nearest-neighbor vacancy jump (to 0.39 eV, as seen in Fig. 10). However unlike the monovacancy case, this barrier is still lower than the barrier for dissociation of the hydrogen atom from the cluster, which we estimate as the incremental binding energy of the hydrogen atom plus its bulk diffusion barrier, yielding a value of 0.64 eV. Following

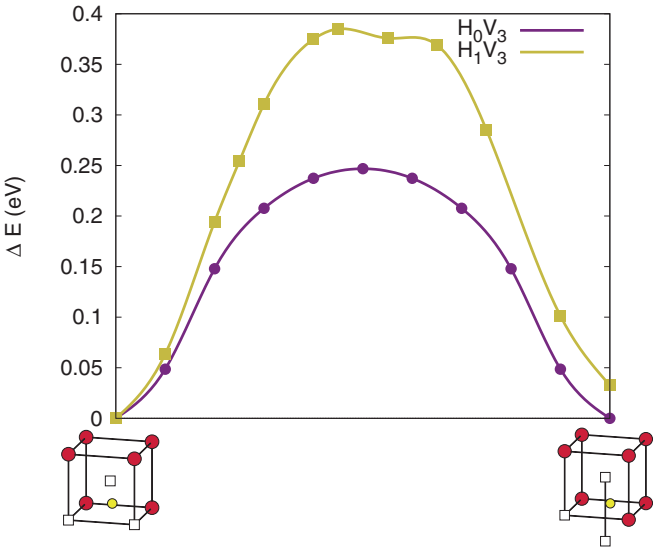

FIG. 10. (Color online) DFT diffusion barriers to a vacancy jump in a trivacancy cluster with and without a hydrogen atom.

the vacancy jump, the hydrogen can make a series of low barrier (all between 0.1 and 0.2 eV) jumps between O sites on the surface of the trivacancy. So, diffusion of a H_1V_3 cluster is likely to proceed by a jump of one of the vacancies, followed by low barrier within-cluster jumps of the hydrogen atom.

The mechanism seen in the trivacancy case allows small clusters of hydrogen and vacancies to migrate without dissociation; however, the trivacancy migrates with an unusually small barrier. If vacancy clusters become less mobile as their size increases,[30,68] then dissociation will be the dominant mechanism for H migration after being trapped in a cluster. Additionally, increasing hydrogen concentration in a cluster may lead to increased barriers to vacancy jumps, but constant or decreased barriers to hydrogen jumps: both of these factors point to hydrogen diffusion by dissociation. We note that in all cases, hydrogen increases the barrier to vacancy diffusion, slowing down the movement of vacancies.

E. Low-energy cluster configurations

Experiments are unable to resolve hydrogen-vacancy clusters in the beginning stages of formation; thus, atomistic simulations provide a valuable tool for investigating the properties of nascent bubbles. We are interested in knowing what cluster shapes are optimal (compact/three-dimensional, planar/two-dimensional, or linear/one-dimensional) and how the preferred shapes may change with the introduction of hydrogen. This information has implications for theories of embrittlement, bubble formation and growth mechanisms, and swelling. While configurations of small clusters of vacancies have been studied before, such as in Beeler and Johnson's[69] lattice model[70] study, there are little data on clusters of more than one vacancy that contain hydrogen.

We use a multiscale approach to model clusters of m hydrogen atoms and n vacancies (H_mV_n). In order to calculate the energetic properties of a cluster, the low energy configuration of the m hydrogen atoms must be known. However, searching for this configuration is nontrivial. Thus, we use the MDMC method described in the methods section to efficiently provide suggestions for low energy configurations. For very small clusters ($n \leqslant 4$), the resulting configurations are further analyzed with SIESTA, along with a few additional intuitively interesting configurations. This allows us to ensure the validity of using the MDMC method to describe larger clusters, which can not be modeled with DFT using available computational resources. Additionally, ZPE corrections are not included in these DFT calculations due to the significant computational resources required. Assuming that ZPE corrections states are within the range of previous calculations (~0.12–0.24 eV/atom), and that we are interested in differences in energies between similar states, the largest possible corrections to the results presented below is expected to be about 0.12 eV. Thus, we expect the contributions for ZPE to be unimportant for determining energetic preference in the majority of cases, with the possible exception of states which are nearly energetically degenerate; this could be applicable to the divacancy and trivacancy cases, but becomes irrelevant as n gets larger.

All very small cluster shapes that were investigated are shown in Figs. 11–13; in each case, they are shown in order from lowest [H_mV_n(a)] to highest energy when $m = 0$. Energy

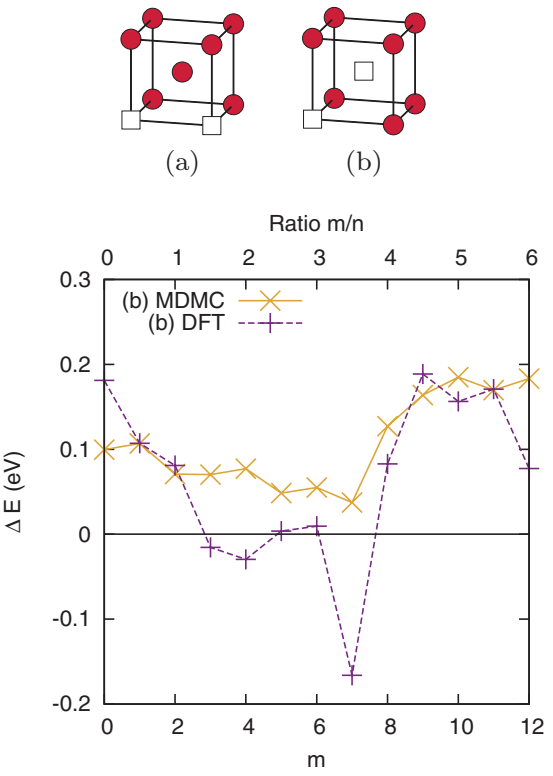

FIG. 11. (Color online) Divacancy clusters are oriented along the (a) ⟨1 0 0⟩ or the (b) ⟨111⟩ direction. The graph shows the difference in energy $\Delta E = E(\text{b}) - E(\text{a})$ as a function of hydrogen concentration, from both MDMC with EAM potential (solid line) and DFT (dotted line).

differences between different configurations with respect to the H_mV_n(a) configurations as a function of hydrogen concentration are shown in Figs. 11–13 for clusters of two, three, and four vacancies, respectively. In general, we find that the vacancy configuration that is the lowest energy when devoid of hydrogen remains the lowest energy when hydrogen is introduced.

As shown in Fig. 11, divacancies may be oriented along the (a) ⟨1 0 0⟩ or the (b) ⟨111⟩ direction. It is generally well known that the ⟨1 0 0⟩ configuration is preferable to the ⟨111⟩; this has been observed recently with DFT calculations,[18,30] and even nearly 50 years ago, Johnson found this to be the preferred configuration using a classical lattice model.[71] However, the effect of adding hydrogen to the clusters is less well studied. Our DFT results show that while the ⟨1 0 0⟩ orientation is usually preferred, there are several hydrogen concentrations that cause the ⟨111⟩ cluster to be lower in energy. Results from MDMC always predict the stability of the ⟨1 0 0⟩ cluster.

As the cluster size increases, hydrogen has less of an effect on the energetic stability. For both the triple and quadruple vacancy clusters, the lowest energy configuration is found to be a compact structure [Figs. 12(a) and 13(a)]. Both MDMC and DFT show that this remains the case even as the hydrogen concentration increases (Figs. 12 and 13).

Tateyama and Ohno show a gain in cluster binding energy when hydrogen hybridizes with iron.[18] This fact, combined with their finding that H_2V_1 complex will be the dominant presence at equilibrium conditions, leads them to suggest that H_2V_1 complexes can be used as building blocks towards larger clusters. To maintain the largest number of hydrogen binding sites, they suggest that tabular or linear configurations

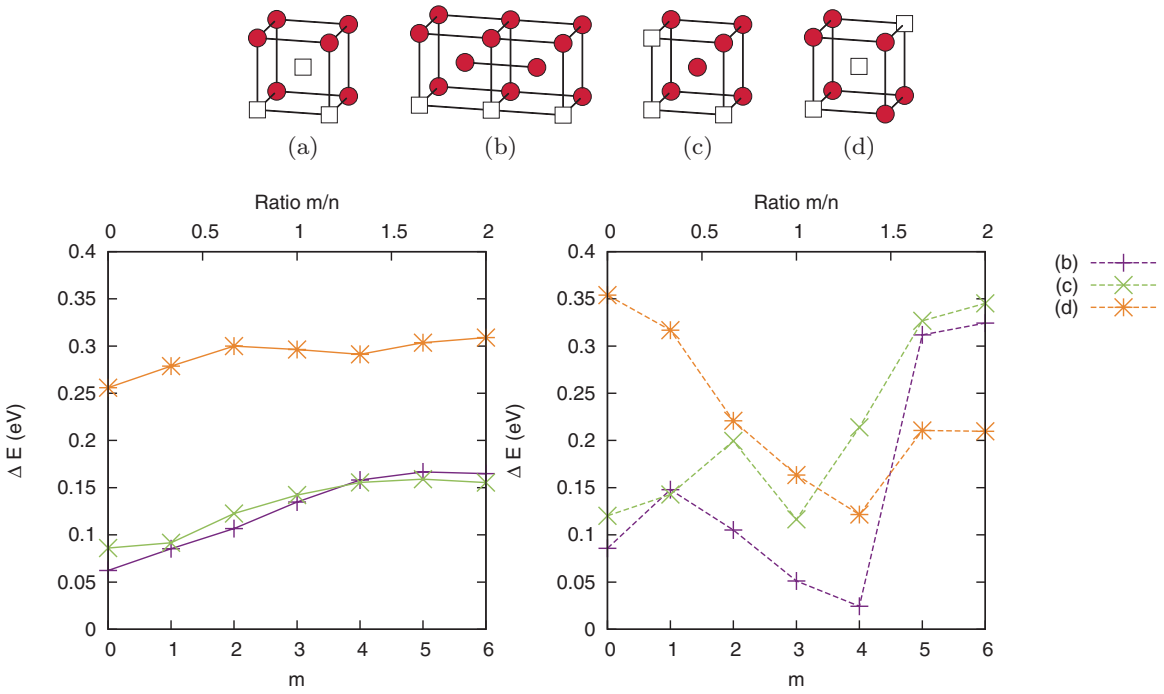

FIG. 12. (Color online) Triple vacancy clusters: The four tested configurations are labeled (a) to (d), in order from the lowest to highest energy. The graphs show the difference in energy ΔE between the configuration (a) and the other configurations as a function of hydrogen concentration. Results using the EAM potential are on the left, the right show results from DFT calculations.

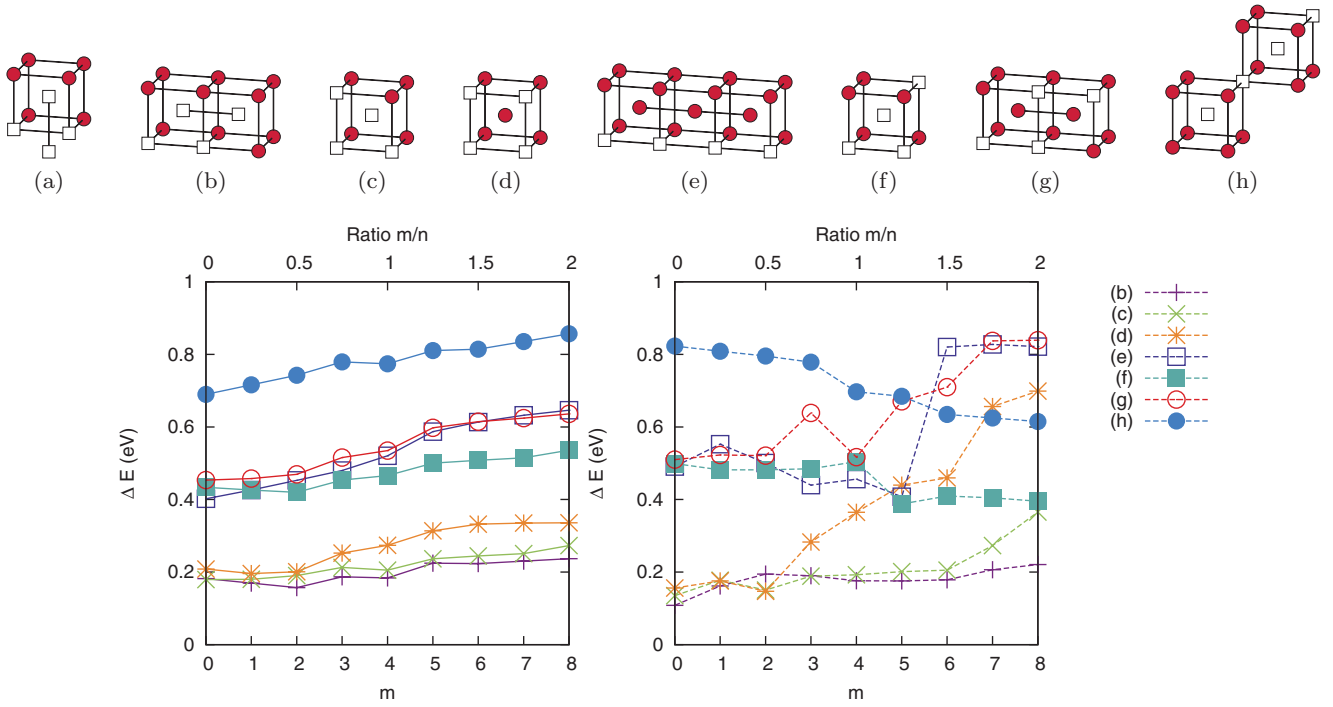

FIG. 13. (Color online) Quadruple vacancy clusters: The eight tested configurations are labeled (a) to (h), in order from the lowest to highest energy. The graphs show the difference in energy ΔE between the configuration (a) and the other configurations as a function of hydrogen concentration. Results using the EAM potential are on the left, the right show results from DFT calculations.

may be most optimal for forming these extended low energy defects. We note that while linear clusters along the ⟨111⟩ direction [H_mV_2(b), H_mV_3(d), and H_mV_4(h)] tend to become relatively more energetically favorable with the addition of hydrogen, we still found that they are among the highest energy configurations tested and become increasingly unfavorable as n increases. Thus, it seems unlikely that extended ⟨111⟩ defects formed of H_2V building blocks will exist. Compact cluster shapes tend to remain the lowest in energy even after the addition of hydrogen.

The incremental binding of vacancies to the lowest energy configuration with $(n-1)$ vacancies is shown in Fig. 14; this binding energy is defined similarly to the hydrogen binding energy of Eq. (4). The binding energy of the vacancy remains roughly constant up to $m/n \simeq 1.5$ (in the undersaturated regime, as discussed below); then it increases linearly with m/n, indicating a vacancy clustering enhancement due to hydrogen. This was previously seen in MD studies[5] and lends support to theories of embrittlement based on vacancy stabilization.

Comparing results from DFT to those found with the EAM potential and LAMMPS, we find good agreement in many cases. For vacancy clusters devoid of hydrogen, the ordering of low to high energy configurations and the magnitude of energy differences between states agrees nearly perfectly with DFT results. As hydrogen is added to the cluster, the EAM potential tends to keep the same relative ordering of configurations, with ΔE increasing as m increases, while DFT results show that there is more detail to the energetic structure of small clusters. Despite some disagreement, especially in the case of trivacancies (Fig. 12), the EAM potential does give a good qualitative, and in many cases quantitative, picture of the relative stability of different configurations.

Based on this success, we rely on the EAM potential to simulate larger clusters that are inaccessible with DFT methods. Spherical clusters are compared with planar clusters; the latter clusters were created by removing a cylinder of atoms with a depth of two lattice planes and relaxing the system, creating a loop structure. The effect of faceting is not considered. While several studies have investigated

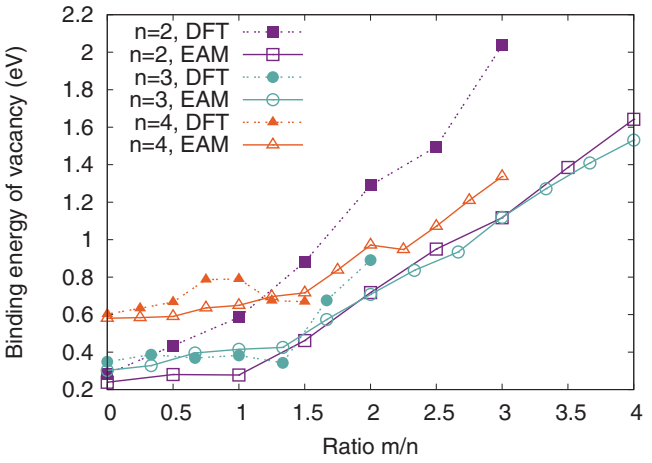

FIG. 14. (Color online) The incremental binding energy of a vacancy to the lowest energy configurations of two, three, and four vacancies as a function of hydrogen to vacancy ratio (m/n). Dotted lines show DFT data; solid lines show data using the empirical potential.

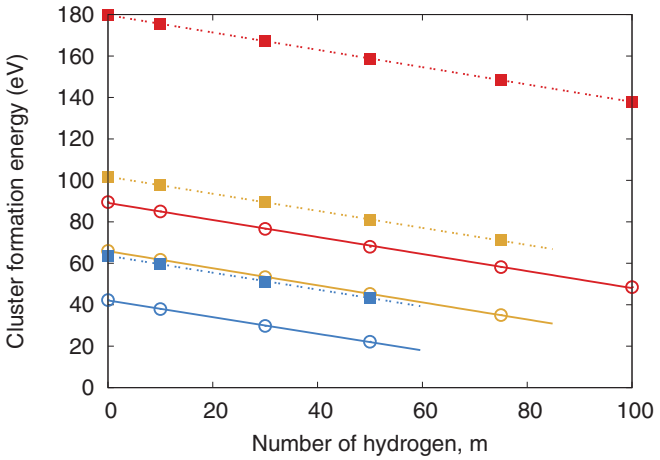

FIG. 15. (Color online) The formation energy of H_mV_n clusters as a function of number of hydrogen atoms m in the undersaturated regime; different curves have different values of n. Data are from MDMC simulations using an empirical potential. Planar cluster curves are indicated by dotted lines with filled square data points, while spherical cluster curves are solid with hollow circle data points. Taking the slope of the lines gives the value of γ used in Eq. (8).

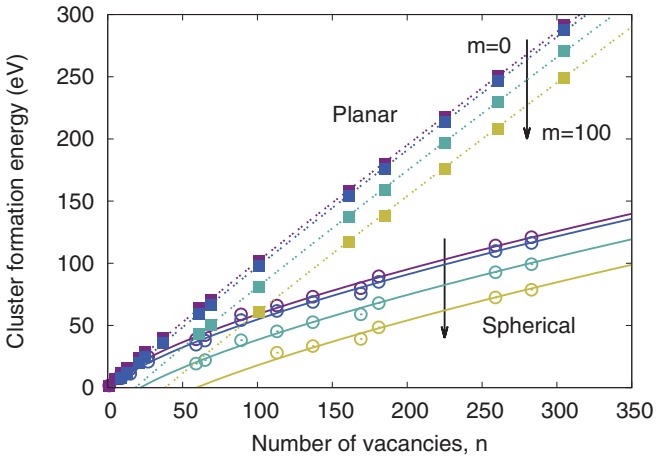

FIG. 16. (Color online) The formation energy of H_mV_n clusters as a function of number of vacancies n in the undersaturated region. The curves are calculated from Eq. (8), while data points are from MDMC simulations using an empirical potential. Planar cluster curves are indicated by dotted lines with filled square data points, while spherical cluster curves are solid with hollow circle data points. The formation energy is also a function of m (curves shown for $m = 0, 10, 50, 100$).

the preferred shape of large voids (devoid of gas),[72–75] the influence of hydrogen has not been previously determined.

Depending on the amount of hydrogen present in a cluster of a given size, we propose that the bubble can be characterized as under or oversaturated. In the undersaturated regime, hydrogen atoms stick to the surface of the bubble, but are far enough apart so that their interactions are negligible. As more hydrogen enters the bubble, the surface becomes saturated, and eventually hydrogen molecules may form in the center. The EAM potential is not suitable for simulating the oversaturated regime, for reasons discussed previously. However in the undersaturated regime, an H_mV_n cluster can be characterized by its formation energy, which is a function of both m and n. We propose the following relationship:

$$E^f(H_mV_n) = \alpha n^\beta + \gamma m. \tag{8}$$

The first term on the right hand side is contributed by the vacancies making up the cluster and reflects the power relationship between the surface area and volume of a void; this form has been successfully used before to describe empty voids.[74,76] The parameters α and β are fit to empty clusters, that is, where $m = 0$. For the spherical clusters, we find values of 2.459 and 0.690 for α and β, respectively. We note that β is extremely close to the expected value for a sphere, $2/3$. For the planar clusters, $\alpha = 1.305$ and $\beta = 0.945$. The second term is due to the presence of hydrogen. In the undersaturated regime, the formation energy of a size n cluster is a decreasing linear function of m, as shown in Fig. 15. Obtaining the slope of a linear fit gives the value of γ; we find that $\gamma = -0.41$ for both cluster shapes. The fact that γ has the same value in all cases supports the idea that hydrogen is essentially noninteracting with other hydrogen atoms. Additionally γ can be related to the incremental binding energy of a hydrogen to the cluster:

$$\begin{aligned} E_B^{\text{inc}} &= E^f(H_{m-1}V_n) - E^f(H_mV_n) + E_{\text{sol}}(H) \\ &= -\gamma + E_{\text{sol}}(H) \end{aligned} \tag{9}$$

where $E_{\text{sol}}(H)$ is the solution energy of hydrogen in iron. With the EAM potential $E_{\text{sol}}(H) = 0.29$ eV and hydrogen atoms have an incremental binding energy of $\sim$0.70 eV. Note that this simple model is valid for small m/n ratios where the incremental vacancy binding energy is roughly constant.

Curves for the formation energy calculated with Eq. (8) and data points from the MDMC simulations are plotted in Fig. 16 for several different hydrogen concentrations; we find excellent agreement between the model and simulation data. In each case, the spherical cluster has a lower formation energy than a comparably sized planar cluster; thus, we expect that spherical clusters will be more energetically favorable than lower dimensional clusters at all sizes in the regime of hydrogen undersaturation. Our results agree well with those of Gilbert *et al.*,[72] who find that spherical configurations are preferred for clusters made up of several hundred vacancies; planar loops are at best metastable, and will eventually decay to spherical clusters by different mechanisms. Although we have only addressed clusters in the unsaturated regime, we speculate that spherical clusters would continue to be energetically preferable to planar clusters as there will be more available volume in which H_2 molecules can form.

IV. CONCLUSION

The behavior of vacancies is affected by the presence of hydrogen, and vice versa. Our atomistic studies, which employ both DFT and MD methods, provide fundamental insight into the causes of these changes. In summary,

(1) Hydrogen resides on T sites in the bulk, but prefers O sites when trapped at vacancies. Changes to hydrogen's electronic structure, including a delocalization of charge, are seen at vacancies. Six hydrogen atoms can be trapped at a monovacancy; the calculated binding energies are in excellent agreement with experiment.

(2) In the bulk, both the $T \rightarrow T$ and the $T \rightarrow O \rightarrow T$ diffusion paths for H have low barriers, at about 0.04 eV, giving diffusion coefficients that are in good agreement with experimental data. The mobility of hydrogen is greatly impeded by the presence of vacancies, due to strong vacancy-hydrogen binding. Reciprocally, the presence of hydrogen also raises barriers to vacancy jumps. Further diffusion of trapped H is expected to occur preferentially by dissociation, with the exception of H_mV_3 clusters, which diffuse with an unusually low barrier of 0.25 eV. The fast diffusion of H_mV_3 without dissociation suggests the ability of vacancies to drag H atoms towards sinks such as dislocations and grain boundaries.

(3) Significantly reduced vacancy formation energies are seen in areas of high local hydrogen concentration, supporting the experimentally observed phenomenon of superabundant vacancy formation.

(4) Incremental binding energy of a vacancy to a H_mV_n cluster remains essentially constant for low m/n ratios, and increases linearly for larger m/n values. Thus, vacancy clustering is clearly enhanced by the presence of significant amount of H atoms.

(5) We propose two extreme regimes of interest for hydrogen bubbles. The strong interaction of hydrogen with iron seen during electronic structure analysis leads to the coating of a H_mV_n cluster surface in the undersaturated regime. Both here and in the bulk, hydrogen atoms do not interact strongly with each other and maintain a minimum interatomic distance of about 1.9 Å. In the oversaturated regime, H_2 molecule formation is possible in the center of clusters.

(6) By fitting to results obtained by the MDMC method on larger clusters, a simple model is proposed to describe cluster formation energy in the undersaturated regime, with low hydrogen-to-vacancy ratio. Here compact or spherical shapes are found to be lower energy structures than planar and linear configurations, for both small and large clusters.

(7) Zero-point energy corrections are important for calculations involving hydrogen. This is particularly true when calculating solution energies and H jump barriers, and less so when calculating binding energies.

ACKNOWLEDGMENTS

This work was supported by French Research National Agency (ANR) in the framework of the HSynThEx project (ANR-10-INTB-0905). All the calculations were performed using resources from HPC-FF (Jülich, Germany) and from GENCI (Grant x2013096020).

[1] R. Oriani and P. Josephic, Acta Metall. **25**, 979 (1977).
[2] H. Birnbaum and P. Sofronis, Mat. Sci. Eng. A **176**, 191 (1994).
[3] M. Nagumo, M. Nakamura, and K. Takai, Metall. Mater. Trans. A **32**, 339 (2001).
[4] M. Nagumo, ISIJ Int. **41**, 590 (2001).
[5] E. Hayward and C. Deo, J. Phys.: Condens. Mat. **23**, 425402 (2011).
[6] T. Neeraj, R. Srinivasan, and J. Li, Acta Mater. **60**, 5160 (2012).
[7] M. Iwamoto and Y. Fukai, Mater. Trans. JIM **40**, 606 (1999).
[8] Y. Fukai, J. Alloy Compound **356-357**, 263 (2003).
[9] S. Myers, P. Richards, W. Wampler, and F. Besenbacher, J. Nucl. Mater. **165**, 9 (1989).
[10] J. Condon and T. Schober, J. Nucl. Mater. **207**, 1 (1993).
[11] F. Garner, E. Simonen, B. Oliver, L. R. Greenwood, M. Grossbeck, W. Wolfer, and P. Scott, J. Nucl. Mater. **356**, 122 (2006).
[12] J. Da Silva and R. McLellan, J. Less-Common Met. **50**, 1 (1976).
[13] H. J. Grabke and E. Riecke, Mater. Tehnol. **34**, 331 (2000).
[14] R. Oriani, Annu. Rev. Mater. Sci. **8**, 327 (1978).
[15] R. Iyer and H. Pickering, Annu. Rev. Mater. Sci. **20**, 299 (1990).
[16] M. Castellote, J. Fullea, P. de Viedma, C. Andrade, C. Alonso, I. Llorente, X. Turrillas, J. Campo, J. Schweitzer, and T. Spillane, Nucl. Instrum. Meth. B **259**, 975 (2007).
[17] D. Nguyen-Manh, A. P. Horsfield, and S. L. Dudarev, Phys. Rev. B **73**, 020101 (2006).
[18] Y. Tateyama and T. Ohno, Phys. Rev. B **67**, 174105 (2003).
[19] D. E. Jiang and E. A. Carter, Phys. Rev. B **70**, 64102 (2004).
[20] B. Irigoyen, R. Ferullo, N. Castellani, and A. Juan, Model. Simul. Mater. Sc. **3**, 319 (2002).
[21] J. Sanchez, J. Fullea, C. Andrade, and P.L. deAndres, Phys. Rev. B **78**, 014113 (2008).
[22] K. Ohsawa, K. Eguchi, H. Watanabe, M. Yamaguchi, and M. Yagi, Phys. Rev. B **85**, 094102 (2012).
[23] E. Hayward, B. Beeler, and C. Deo, Phil. Mag. Lett. **92**, 217 (2012).
[24] W. A. Counts, C. Wolverton, and R. Gibala, Acta Mater. **58**, 4730 (2010).
[25] J. M. Soler, E. Artacho, J. D. Gale, A. Garc, J. Junquera, P. Ordejón, and D. Sánchez-Portal, J. Phys.: Condens. Mat. **14**, 2745 (2002).
[26] J. P. Perdew, K. Burke, and M. Ernzerhof, Phys. Rev. Lett. **77**, 3865 (1996).
[27] A. T. Paxton, M. Methfessel, and H. M. Polatoglou, Phys. Rev. B **41**, 8127 (1990).
[28] G. Y. Guo and H. H. Wang, Chinese J. Phys. **38**, 949 (2000).
[29] J. Hafner, Acta Mater. **48**, 71 (2000).
[30] C.-C. Fu, J. Dalla Torre, F. Willaime, J. Bocquet, and A. Barbu, Nat. Mater. **4**, 68 (2005).
[31] C.-C. Fu and F. Willaime, Phys. Rev. B **72**, 064117 (2005).
[32] C.-C. Fu and F. Willaime, J. Nucl. Mater. **367-370**, 244 (2007).
[33] K. K. Irikura, J. Phys. Chem. Ref. Data **36**, 389 (2007).
[34] National Institute of Standards and Technology Computational Chemistry Comparison and Benchmark DataBase, http://cccbdb.nist.gov/.
[35] M. Methfessel, M. van Schilfgaarde, and M. Scheffler, Phys. Rev. Lett. **70**, 29 (1993).
[36] C. J. Pickard and R. J. Needs, Nat. Phys. **3**, 473 (2007).
[37] C. Wolverton, V. Ozolins, and M. Asta, Phys. Rev. B **69**, 144109 (2004).
[38] S. Plimpton, J. Comput. Phys. **117**, 1 (1995).
[39] M. S. Daw and M. I. Baskes, Phys. Rev. B **29**, 6443 (1984).
[40] A. Ramasubramaniam, M. Itakura, and E. A. Carter, Phys. Rev. B **79**, 174101 (2009).
[41] A. Ramasubramaniam, M. Itakura, and E. A. Carter, Phys. Rev. B **81**, 099902 (2010).

[42]N. Metropolis, A. Rosenbluth, M. Rosenbluth, A. Teller, and E. Teller, J. Chem. Phys. **21**, 1087 (1953).
[43]G. Henkelman, B. P. Uberuaga, and H. Jonsson, J. Chem. Phys. **113**, 9901 (2000).
[44]F. Soisson and C.-C. Fu, Phys. Rev. B **76**, 214102 (2007).
[45]E. Meslin, C.-C. Fu, A. Barbu, F. Gao, and F. Willaime, Phys. Rev. B **75**, 094303 (2007).
[46]K. Kiuchi and R. B. Mclellan, Acta Metall. **31**, 961 (1983).
[47]K. Heinola and T. Ahlgren, J. Appl. Phys. **107**, 113531 (2010).
[48]A. Moitra and K. Solanki, Comp. Mater. Sci. **50**, 2291 (2011).
[49]D. F. Johnson and E. A. Carter, J. Mater. Res. **25**, 315 (2011).
[50]C. Ouyang and Y.-S. Lee, Phys. Rev. B **83**, 045111 (2011).
[51]P. G. Sundell and G. Wahnstrom, Phys. Rev. B **70**, 224301 (2004).
[52]J. P. Hirth, Metall. Mater. Trans. A **11A**, 861 (1980).
[53]K. Miwa and A. Fukumoto, Phys. Rev. B **65**, 155114 (2002).
[54]H. Eyring, Trans. Faraday Soc. **34**, 41 (1938).
[55]E. Wigner, Trans. Faraday Soc. **34**, 29 (1938).
[56]K. W. Kehr, in *Hydrogen in Metals I* (Springer, Berlin, 1978), p. 197.
[57]J. Murrell and K. Laidler, Trans. Faraday Soc. **64**, 371 (1968).
[58]D. J. Wales and R. S. Berry, J. Chem. Soc. Faraday Trans. **88**, 543 (1992).
[59]D. J. Wales, *Energy Landscapes* (Cambridge University Press, Cambridge, 2003), pp. 192–196.
[60]Y. Hayashi and W. Shu, Solid State Phen. **73-75**, 65 (2000).
[61] H. Hagi, Mater. Trans. JIM **35**, 112 (1994).
[62]Y.-W. You, X.-S. Kong, X.-B. Wu, Q. F. Fang, J.-L. Chen, G.-N. Luo, and C. Liu, J. Nucl. Mater. **433**, 167 (2013).
[63]Y. L. Liu, Y. Zhang, H. B. Zhou, G. H. Lu, F. Liu, and G. N. Luo, Phys. Rev. B **79**, 172103 (2009).
[64]S. Myers, D. Follstaedt, F. Besenbacher, and J. Bøttiger, J. Appl. Phys. **53**, 8734 (1982).
[65]F. Besenbacher, S. Myers, P. Nordlander, and J. Nørskov, J. Appl. Phys. **61**, 1788 (1987).
[66]H. Amara, C.-C. Fu, F. Soisson, and P. Maugis, Phys. Rev. B **81**, 174101 (2010).
[67]Fu *et al*., find diffusion barriers of 0.62, 0.35, and 0.48 eV for the V_2, V_3, and V_4 clusters, respectively, compared to 0.68 eV for the monovacancy jump.[30] The quantitative differences between our results and theirs can be explained partially by the size effect (we use a 250 atom cell compared to theirs with 128) and partially as a difference in the basis set.
[68]Y. Fan, A. Kushima, S. Yip, and B. Yildiz, Phys. Rev. Lett. **106**, 125501 (2011).
[69]J. R. Beeler and R. A. Johnson, Phys. Rev. **156**, 677 (1967).
[70]R. A. Johnson and E. Brown, Phys. Rev. **127**, 446 (1962).
[71]R. A. Johnson, Phys. Rev. **134**, A1329 (1964).
[72]M. R. Gilbert, S. L. Dudarev, P. M. Derlet, and D. G. Pettifor, J. Phys.: Condens. Mat. **20**, 345214 (2008).
[73]Y. N. Osetsky, D. J. Bacon, A. Serra, B. Singh, and S. Golubov, J. Nucl. Mater. **276**, 65 (2000).
[74]N. Soneda and T. Diaz de la Rubia, Philos. Mag. A **78**, 37 (1998).
[75]C. C. Matthai and D. J. Bacon, J. Nucl. Mater. **135**, 173 (1985).
[76]R. Wagner and R. Kampmann, *Materials Science and Technology: A Comprehensive Treatment*. *Phase Transformations in Materials*, Materials Science and Technology, Vol. 5 (VCH, Weinheim, 1991), p. 243.